NUMERICAL SIMULATION OF CU-RICH PRECIPITATE EVOLUTION IN CU-BEARING 316L AUSTENITIC STAINLESS STEEL

Q. XIONG*, J. D. ROBSON*, T. F. FLINT*, Y. SUN,
A. N. VASILEIOU* and M. C. SMITH*

**School of Mechanical, Aerospace and Civil Engineering, The University of Manchester*

DOI 10.3217/978-3-85125-615-4-14

ABSTRACT

A numerical model based on the coupling of the thermodynamic software ThermoCalc and the Kampmann and Wagner Numerical (KWN) framework has been developed in this work to predict the evolution of Cu-rich precipitates in 316 stainless steels. The effect of precipitation hardenning on mechanical properties at 700°C is investigated as well. The predicted average particle size, volume fraction and number density of precipitates agree well with the experimental observations. In addition, the precipitation strengthening effects of Cu-rich precipitates were quantitatively evaluated and agree with experimental data as well. The slow increase in average radius of Cu-rich precipitates was consistent with the modest change in yield strength with extended aging. These cumulative results and analyses could provide a solid foundation for much wider applications of Cu-bearing stainless steels. The developed model can be used to predict the precipitation behaviour in other similar austenitic stainless steels.

Keywords: Cu-rich precipitates, 316 stainless steel, modelling

INTRODUCTION

The outstanding mechanical formability, good high temperature strength and oxidation resistance of AISI 316 austenitic stainless steels make them widely used materials in nuclear power plants [1]. However, the degradation of these materials can result from thermal aging and other external factors (irradiation, stress, temperature, coolant media, etc.), which could affect the reliability of components [2, 3]. After heat treatment, Cu-rich precipitates in the steel matrix will be produced if sufficient amount of copper is present in the steel. It is well known that the stability, size, type and number density of Cu-rich precipitates are mainly attributed to superior antibacterial property to the stainless steel and high temperature strength improvement [6-9]. The stability of these phases in multicomponent materials such as AISI 316SS under thermal aging is affected by many variables such as alloy composition, temperature, time, and processing history. However, there is currently a lack of in-depth understanding of Cu precipitation behaviour in austenitic steels [10].

Several investigations have reported Cu-rich precipitation during isothermal heat treatment and its effects on mechanical properties in austenitic stainless steel [2, 9-11], but clearly there are practical limits to the duration of such experiments. To be able to extrapolate these results to longer timeframes, a numerical method is required to predict precipitate evolution. The simulation of Cu-rich precipitation requires a suitable modelling framework for capturing the complexity of the multicomponent system and involving the simultaneous occurrence of nucleation, growth and coarsening. Many efforts have been devoted to the modelling of the microstructure during the precipitation process for different types of materials [12, 13]. Accurate modelling of the precipitation process requires a synchronous consideration of all these contributions to simulate the temporal evolution of microstructure. Moreover, the phase equilibrium information as well as the composition and mobility data of the matrix phase need to be constantly updated as nucleation, growth and coarsening proceed. Therefore, a smooth integration of thermodynamic calculation, kinetic simulation and property modelling of the material is necessary. However, an integrated framework coupling reliable thermodynamic calculation, kinetic simulation and property prediction of 316SS is rarely available.

In this work, the ThermoCalc and Kampmann and Wagner approach (KWN model) are combined to predict the phase stability, phase compositions and precipitation. First, the phase properties under different compositions and temperatures are calculated from ThermoCalc. These may then be used as inputs for the precipitation kinetics and accelerate the understanding of the stability of precipitate phases in 316SS steels under extended thermal aging [14]. The simulation results demonstrate the potential applications of the current methodology to the understanding of phase stability in similar structural materials. The KWN model is used to predict the precipitation behaviour, and can deal with nucleation-growth-coarsening phenomena within the same formulation. A few models based on this framework have been applied to a number of systems [12, 15, 16]. An important limitation in those approaches is that the overall kinetics is computed by imposing a constant concentration at the precipitate/matrix interface, and by employing a driving force obtained from binary dilute solution approximation. Because of the decrease of solute supersaturation in the matrix during precipitation, the local equilibrium concentration at the precipitate/matrix interface may change significantly. Moreover, the chemical free energy change during nucleation based on the dilute solution approximation in high-alloy systems is also not precise, especially for ternary or higher order systems. The model presented here intends to overcome this problem via computing multicomponent thermodynamic equilibrium in the time domain, to obtain the instantaneous local equilibrium condition at the matrix/precipitate interface during precipitation. Homogeneous precipitation is considered in this work. The results of this model show good agreement with experimental observations for late precipitation stages. The precipitation behaviour of Cu-rich particles in 316SS is thus well understood. The effects of the precipitation on the mechanical properties are studies as well.

MATERIAL DETAILS AND EXPERIMENTAL DATA

SAMPLES

The chemical composition of the Cu-bearing 316 L austenitic stainless steel (SS) investigated in this work is shown in Table 1.

Table 1. Composition (wt%) of 316LCu alloy with Fe as balance

Alloy	C	P	S	Cr	Ni	Mo	Cu
316LCu	0.016	0.005	0.001	18.18	14.5	3.02	4.36

EXPERIMENTAL DATA

Tong Xi etc. solution-treated the 316L-Cu specimens at 1100 °C for 30 min, followed by water quenching. The specimens were then aged isothermally at 700 °C for 20 min, 3 h, 6 h, 10 h, and 15 h, respectively. TEM (transmission electron microscopy) was used to analyse the morphology, size and the orientation relationship of Cu-rich precipitates in the 316L-Cu SS. APT (atom probe tomography) was used to characterize the evolution and calculate the size of Cu-rich precipitates [17]. The experimental results show that, with increasing aging time, the spherical morphology of Cu-rich precipitate remains unchanged. Moreover, the lattice constant of the austenitic matrix after solid solution treatment is very close to that of the FCC Cu-rich precipitates, and the lattice constant misfit $\Delta\alpha/\alpha$ is small [24, 25]. The composition of Cu-rich precipitates obtained by proxigram analysis was 94.1671.26 at.% Cu and 1.7870.22 at.% Fe after 20 min aging, 98.0471.94 at.% Cu and 1.9671.92 at.% Fe after 6 h aging, and 99.1770.82 at.% Cu and 0.8370.81 at.% Fe after 15 h aging.

The average radius increased slightly from 1.38 nm to 2.39 nm as the aging time increased. The relatively slow growth and coarsening behaviour of Cu-rich precipitates was largely attributed to the slower diffusion kinetics of Cu than Fe, low interfacial energy and high strain energy of Cu-rich precipitates in the austenite matrix [17]. The measured average radius, number density, and volume fraction Φ of the Cu-rich precipitates as a function of aging time will be compared with calculated results in the next section.

THERMODYNAMIC RESULTS

To produce a reliable kinetic model, it is first necessary to have a sufficient understanding of the phase equilibrium of the system being modelled. Quantities such as equilibrium solubility and driving forces must be predicted and used as inputs to the kinetic model. The ThermoCalc® software [20] employing the TCFE8 thermodynamic database was used to calculate phase stabilities and compositions. This produces the solute concentration in the matrix (α) and in the precipitate (β) under equilibrium. In addition, the chemical potentials of all the components are obtained and employed to determine the chemical driving force for the nucleation of the precipitates.

The calculated equilibrium phases and their mole fractions in 316LCu are demonstrated in Fig.1. Here, the open symbols denote the precipitate phases while the solid symbols denote the matrix phase in 316LCu. The main precipitates are sigma, $M_{23}C_6$, HCP, Laves and Cu-rich precipitate.

The predicted composition of precipitate phases is shown in Fig.2 and is compared with experimental results. The predicted equilibrium Cu-rich precipitates contain 94.02 at% Cu, and 0.516 at% Fe. While the Cu-rich precipitates obtained by proxigram analysis contain 94.167±1.26 at.% Cu and 1.787±0.22 at.% Fe, 98.047±1.94 at.% Cu and 1.967±1.92 at.% Fe and 99.177±0.82 at.% Cu and 0.837±0.81 at.% Fe after 20 min, 6 h and 15 h aging, respectively. The agreement between the calculated and experimental results are reasonable.

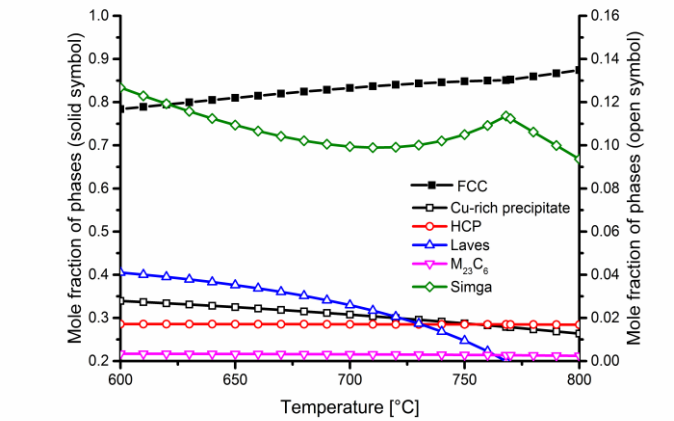

Fig.1 Calculated equilibrium phase mole fraction vs temperature for 316LCu

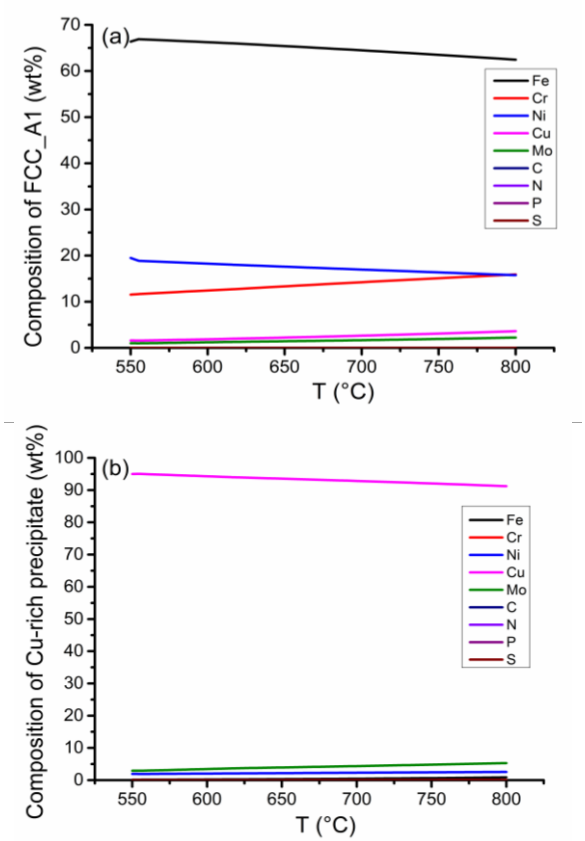

Fig.2 Calculated phase compositions in 316LCu for (a) FCC_A1 (b) Cu-rich precipitate

PRECIPITATION KINETICS SIMULATION

The preferred nucleation sites of precipitate phases were specified based on experimental evidence. In 316LCu, high number densities of spheroidal Cu-rich precipitates were homogeneously distributed in the austenitic matrix and the interface between Cu-rich precipitates and austenitic matrix remained coherent during the aging process [2, 17].

In this work, the KWN model is applied to predict precipitation of multiple phases [16]. The process of nucleation, growth, and coarsening of particles can be predicted simultaneously in this model. The number of new Cu-rich precipitates is calculated according to classical nucleation theory. The growth of particles is assumed to be governed by the diffusion rate of Cu to or from the particle/matrix interface. The particle size distribution and the volume fraction of the precipitate particles are updated at each time step. They are used to recalculate the matrix compositions during discrete time steps which are determined by a mean-field approach. After each time-step, the Cu concentration remaining in the matrix is recalculated and used in the next time-step. Coarsening arises naturally in the model. Using this method, the transition from nucleation and growth to a

coarsening-dominated regime is naturally predicted as the precipitate volume fraction increases.

NUCLEATION

Classical nucleation theory gives the homogeneous nucleation rate as [15]:

$$I = N_v Z \beta^* \exp\left[-\frac{4\pi\gamma_n r^{*2}}{3kT}\right]\exp\left(-\frac{\tau}{t}\right) \quad (1)$$

where N_v is the number of nucleation sites per unit volume (equal to the number of atoms per volume for homogeneous nucleation);

Z is the Zeldovich nonequilibrium factor, $Z = \frac{V_a \Delta G_v^{\ 2}}{8\pi\sqrt{\gamma_n^3 kT}}$;

β^* is the rate of atomic attachment to a growing embryo, $\beta^* = 16\pi\gamma_n^2 cD / \Delta G_v^{\ 2} a^4$;

k is the Boltzmann constant;

T is the thermodynamic temperature;

γ_n is the interfacial energy of the matrix/nucleus interface; The interfacial energy of Cu-rich precipitated is cited from [11, 20].

r^* is the radius of the critical nucleus, $r^* = -2\gamma_n / \Delta G_v$;

τ is the incubation time for nucleation, $\tau = 8kT\gamma_n a^4 / V_a^2 \Delta G_v Dc$;

ΔG_v is the chemical volume free energy change driving nucleation,

$$\Delta G_v = -\frac{RT}{V_m}\left[c_e^{\beta}\frac{\ln(c_i)}{\ln(c_e^{\alpha})} + (1-c_e^{\beta})\frac{\ln(1-c_i)}{\ln(1-c_e^{\alpha})}\right];$$

V_m is the molar volume of the precipitating phase;

c_i is the instantaneous concentration of Cu in the matrix. This is the far field matrix concentration, strictly speaking an infinite distance from the precipitate/matrix interface;

c^{α}_e is the concentration of solute in the matrix (α) in equilibrium with the precipitate (β);

c^{β}_e is the equilibrium concentration of solute in the precipitate phase;

V_a is the volume per atom in the matrix;

c is the concentration (atomic fraction) of Cu solute in the matrix;

a is the lattice constant of the product phase which is equal to 0.36 nm in this work [10];

D is the diffusivity of Cu precipitate in matrix.

GROWTH

The Cu-rich particles appear approximately spherical in shape. The modelling of precipitate growth with local equilibrium at the interface is based on the theory for spherical precipitates. The development of the radius of the spherical precipitate is assumed to follow the parabolic equation. The growth rate is limited by the rate at which Cu can diffuse to the particles and is given by

$$\frac{dr}{dt} = \frac{D}{r}\frac{c_i - c_r^{\alpha}}{c^{\beta} - c_r^{\alpha}} \tag{2}$$

where D is the chemical diffusion coefficient of Cu [m2/s], r is the particle radius [m], c_r^{α} is the concentration of solutes in the matrix at the interface (which depends on the particle radius due to the effect of capillarity), c^{β} is the concentration of solute in precipitates and ci is the instantaneous concentration of Cu in the matrix. $c_r^{\alpha}$is calculated using the Gibbs–Thomson equation:

$$c_r^{\alpha} = c_{\infty}^{\alpha} \exp\left(\frac{2\gamma_n V_m}{RT}\frac{1}{r}\right) \tag{3}$$

where γ_n is the interfacial energy of the growing (or shrinking) particle [J/m^2].

The mean solute concentration of the components in the matrix, c_i, is updated after each time step:

$$c_i = c_0 - (c^{\beta} - c^{\alpha})\int_0^{\infty}\frac{4}{3}\pi r^3 \phi dr \tag{4}$$

where ϕ is the size distribution function. The newly obtained multicomponent matrix composition is employed as an input for the thermodynamic computations in the next time step.

The chemical diffusion coefficient of Cu in γ-iron is measured in [18]

$$D = 0.19\exp\left(\frac{-65100}{RT}\right)\times 10^{-4} \tag{5}$$

PRECIPITATE COARSENING

Coarsening occurs when large precipitates grow at the expense of small ones, without a change the overall volume fraction. As the fraction of solute in the matrix decreases during precipitation, the driving force for nucleation and growth of the precipitate particles decreases and the critical particle radius increases. The growth rates of all the particles size classes were calculated at the edges (i.e. upper and lower bounds) of each class. For particles with radii smaller than the critical radius, r∗, the size of the particles will have a negative growth rate according to Eq.(2). Particles radii larger than r∗ will retain a positive growth rate and increase in size. When the size of a group of shrinking particles reaches zero they are removed from the size distribution. The particles are then reallocated to the size classes.

Secondly, the precipitates size distribution at each iteration is updated by a third order Runge–Kutta scheme [19] with an adaptive time step. The time step was adjusted to ensure that the error in the change in radius was less than 0.1 nm between steps and the error in the prediction of number density was less than 0.01 particle/μm3. In the early stages of precipitation, the time step is very small to ensure these criteria are met when nucleation and growth rates are most rapid. In the later stages of precipitation and during coarsening, the time step expands, where changes occur more slowly, allowing more efficient calculation.

Table 2 Parameters used in this work

Parameter	value	Reference
N_v		Calculated in this work
a	0.36e-9 m	[20]
γ_n	0.017 J/m^2	[11, 20]
V_m	7.457e-6 m^3/mol	Calculated by Thermo-Calc
V_a	1.17×10^{-29} m^3	[21]
k	1.38×10^{-23} m^2*kg/(s^2*K)	[22]
R	8.314 J/(mol*K)	[22]
T	700 °C	In this work
M	3	Taylor factor
G	75.3GPa	Shear modulus
b	0.254nm	Burgers vector
$\Delta a/a$	0.38%	Misfit parameter

STRENGTH MODEL

The increment of macroscopic yield strength σ_p can be calculated as [10]

$$\sigma_p = 4.1MG\varepsilon^{3/2}v_f^{1/2}(\frac{R}{b})^{1/2} + \frac{2M}{bLT^{1/2}}(\gamma_n b)^{2/3} \quad (6)$$

where M is the Taylor factor, G is the shear modulus of the austenitic matrix and b is the Burgers vector in the matrix , T is the line tension of the dislocation, approximately equal to $Gb^2/2$ [49], $\varepsilon = 2/3\ (\Delta a/a)$ is the coherency strain, $L=0.866/(RN)^{1/2}$ is the mean particle spacing in the slip plane, v_f , N and R are the volume fraction, number density and average radius of Cu-rich precipitates, respectively. These input parameters are shown in Table 2.

RESULTS AND DISCUSSION

The integrated model can now be used to predict precipitation for a range of alloy compositions and investigate the effect of changing the bulk alloy composition on the precipitation kinetics. The input parameters are shown in Table 2. Fig. 3 shows plots of the predicted evolution of volume fraction, number density and particle radius along with the experimental data at 700°C. The average measured radius of Cu-rich precipitates is 1.387±0.46 nm after aging for 20min, while it increased to 2.077±0.71nm and 2.397±0.81 nm after aging for 6h and 15h, respectively. Meanwhile, the number density of the Cu-rich precipitate decreases continuously from 1.29×10^{24} m^{-3} after 20 min aging to 4.27×10^{23} m^{-3} after 6h aging and further to 2.65×10^{23} m^{-3} after 15h aging [10]. The predicted radius of Cu-rich precipitates is 1.4 nm after aging for 20min, while it increased to 2.0 nm and 2.4 nm after aging for 6h and 15h, respectively. The predicted number density of the Cu-rich precipitate decreases continuously from 1.3×10^{24} m^{-3} after 20 min aging to 4.3×10^{23} m^{-3} after 6h aging and further to 2.7×10^{23} m^{-3} after 15h aging.

The predicted volume fraction, number density and average size of Cu-rich particles are in good agreement with published experimental results. The volume fraction of Cu-rich particles increases rapidly initially and then remains relatively constant at different aging time, indicating that the Cu-rich precipitates are in a regime where growth and coarsening are dominant. At first, the number density of Cu-rich particles increases rapidly in a very short time. Then the number density begins to decrease as described by the experiment. The decrease of number density is very fast and followed by a relatively stable state. Meanwhile, the average precipitate size increased with increasing the aging time. After increasing rapidly in size at the early stage of aging, the growth rate of Cu-rich particles slowed down and kept at a relatively stable state. The slight increase in mean radius and decrease in number density were consistent with the tiny change in mechanical properties under different aging time [10].

The predicted total precipitation strengthening is shown in Fig.4, which is 15.81MPa, 20.37MPa and 21.23MPa for 20min, 6h and 15h aging, respectively. The calculated results are a bit higher than the experimental results but within reasonable agreements. The reason resulting in the slowly increment of yield strength with extended aging time is the weak precipitation strengthening effect of Cu-rich precipitate and the slow growth of the Cu-rich precipitate.

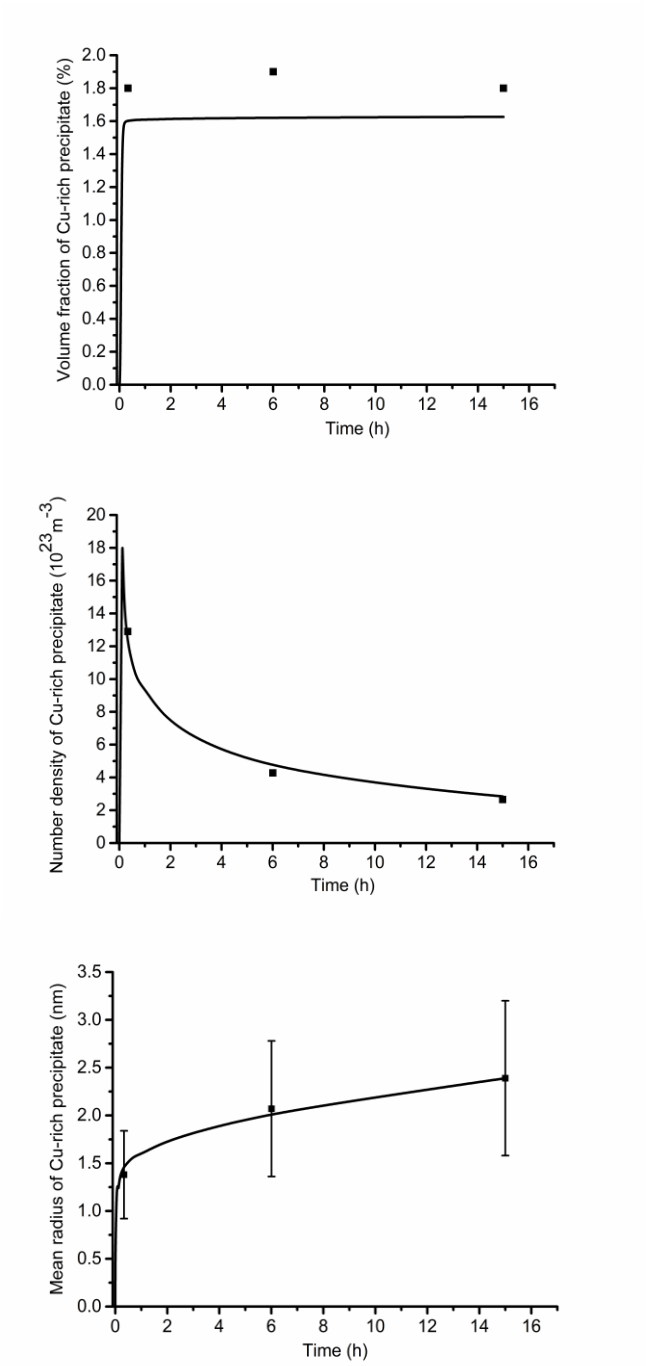

Fig. 3. Predicted and measured evolution of: (a) volume fraction of Cu-rich precipitate (b) Cu-rich precipitate number density; and (c) mean radius with time at 700°C. Measured data from [17]

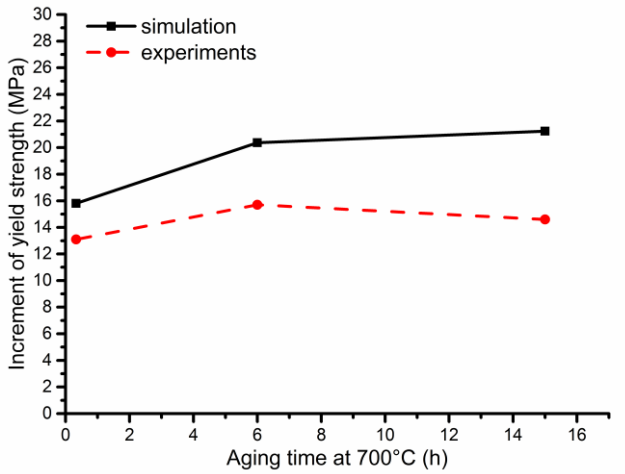

Fig. 4. Strengthening contributions of Cu-rich precipitates in316L-CuSS.

CONCLUSIONS

A model describing the precipitation kinetics is developed. The model is based on a KWN framework with continuous nucleation in the matrix and a growth rate computation incorporating capillarity effects. The model is coupled with ThermoCalc® thermodynamic databases for obtaining the instantaneous equilibrium condition at interface. Models have been developed to predict the full precipitation process for the Cu-rich precipitate phase, from the initial nucleation stage to the final coarsening dominated stage. The size distributions and particle size evolution predicted by the model in this study agree well with the experimental data reported in the literature. The model is able to predict the overlapped nucleation-growth-coarsening kinetics in a natural way and trace the particle size distribution throughout the process. The model is of a general nature, and it can be applied to other precipitate phases present in similar stainless steels. The precipitation hardening effects of Cu-rich precipitates are simply and quantitatively analysed. The strengthening effects are found to be relatively small and consistent with the experimental results.

ACKNOWLEDGEMENTS

The authors gratefully acknowledge the contributions of all the participants in this work. The support of the UK Engineering and Physical Sciences Research Council for M C Smith is also acknowledged, via the Fellowship in Manufacturing “A whole-life approach to the development of high integrity welding technologies for Generation IV fast reactors”, EP/L015013/1. The authors acknowledge the use of the EPSRC-funded JEOL JXA-8530F FEG-EPMA, award EP/M028097/1.

REFERENCES

[1] MAZIASZ, P. and J. BUSBY: *Properties of austenitic steels for nuclear reactor applications*, in *Comprehensive Nuclear Materials*. 2012, Elsevier Oxford. p. 267-283.

[2] SAHLAOUI, H., ET AL., *Effects of ageing conditions on the precipitates evolution, chromium depletion and intergranular corrosion susceptibility of AISI 316L: experimental and modeling results.* Materials Science and Engineering: A, 2004. 372(1–2): p. 98-108.

[3] MAZIASZ, P.J.: *Overview of microstructural evolution in neutron-irradiated austenitic stainless steels.* Journal of Nuclear Materials, 1993. 205: p. 118-145.

[4] REN, L., ET AL.: *Preliminary study of anti-infective function of a copper-bearing stainless steel.* Materials Science and Engineering: C, 2012. 32(5): p. 1204-1209.

[5] XI, T., ET AL., *Study of the processing map and hot deformation behavior of a Cu-bearing 317LN austenitic stainless steel.* Materials & Design, 2015. 87: p. 303-312.

[6] ARGON, A.: *Strengthening mechanisms in crystal plasticity*. 2008: Oxford University Press on Demand.

[7] MULHOLLAND, M.D. and D.N. SEIDMAN: *Nanoscale co-precipitation and mechanical properties of a high-strength low-carbon steel.* Acta Materialia, 2011. 59(5): p. 1881-1897.

[8] JIAO, Z.B., ET AL.: *Precipitation mechanism and mechanical properties of an ultra-high strength steel hardened by nanoscale NiAl and Cu particles.* Acta Materialia, 2015. 97: p. 58-67.

[9] PADILHA, A.F., ET AL.: *Precipitation in AISI 316L(N) during creep tests at 550 and 600 °C up to 10 years.* Journal of Nuclear Materials, 2007. 362(1): p. 132-138.

[10] XI, T., ET AL.: *Copper precipitation behavior and mechanical properties of Cu-bearing 316L austenitic stainless steel: A comprehensive cross-correlation study.* Materials Science and Engineering: A, 2016. 675: p. 243-252.

[11] HONG, Y.J.O.J.H.: *Nitrogen effect on precipitation and sensitization in cold-worked Type 316L(N) stainless steels.* Journal of Nuclear Materials, 2000. 278: p. 242-250.

[12] ROBSON, J.D.: *Modelling the overlap of nucleation, growth and coarsening during precipitation.* Acta Materialia, 2004. 52(15): p. 4669-4676.

[13] KOZESCHNIK, E., ET AL.: *Modelling of kinetics in multi-component multi-phase systems with spherical precipitates: II: Numerical solution and application.* Materials Science and Engineering: A, 2004. 385(1–2): p. 157-165.

[14] ANDERSSON, J.O., ET AL.: *Thermo-Calc & DICTRA, computational tools for materials science.* Calphad: Computer Coupling of Phase Diagrams and Thermochemistry, 2002. 26(2): p. 273-312.

[15] ROBSON, J.D., M.J. JONES, and P.B. PRANGNELL: *Extension of the N-model to predict competing homogeneous and heterogeneous precipitation in Al-Sc alloys.* Acta Materialia, 2003. 51(5): p. 1453-1468.

[16] ROBSON, J.D.: *A new model for prediction of dispersoid precipitation in aluminium alloys containing zirconium and scandium.* Acta Materialia, 2004. 52(6): p. 1409-1421.

[17] LAI, J.K.L.: *A review of precipitation behaviour in AISI type 316 stainless steel.* Materials Science and Engineering, 1983. 61(2): p. 101-109.

[18] SALJE, G. and M. FELLER KNIEPMEIER: *The diffusion and solubility of copper in iron.* Journal of Applied Physics, 1977. 48(5): p. 1833-1839.

[19] ROBSON, J.D. and P.B. PRANGNELL: *Modelling Al3Zr dispersoid precipitation in multicomponent aluminium alloys.* Materials Science and Engineering: A, 2003. **352**(1–2): p. 240-250.

[20] LEWIS, M.H. and B. HATTERSLEY: *Precipitation of M23C6 in austenitic steels.* Acta Metallurgica, 1965. 13(11): p. 1159-1168.

[21] LEE, E., P. MAZIASZ, and A. ROWCLIFFE, *Structure and composition of phases occurring in austenitic stainless steels in thermal and irradiation environments*. 1980, Oak Ridge National Lab., TN (USA).

[22] CHRISTIAN, J.W.: *The Theory of Transformations in Metals and Alloys*, in *The Theory of Transformations in Metals and Alloys*. 2002, Pergamon: Oxford. p. ix.